Semnan University

Mechanics of Advanced Composite Structures

journal homepage: http://MACS.journals.semnan.ac.ir

The Graft of ANN-FEM Technique in Macro-mechanics of Multi-oriented Natural Fiber/Polyester Laminates

C. Emeka Okafor [a]*, C. Chukwutoo Ihueze [b]

[a]*Department of Mechanical Engineering, Nnamdi Azikiwe University, Awka, Nigeria*
[b]*Department of Industrial and Production Engineering, Nnamdi Azikiwe University, Awka, Nigeria*

KEYWORDS

Laminate Ply Forces
Macro-mechanical Analysis
Plantain Fiber Composite
Artificial Neural Network
Finite Element Method

ABSTRACT

Low weight and high strength requirements are prime target design objectives in strength demanding applications. Skillful design of low density, low weight and eco-friendly natural fiber composites could provide an alternative material route to the actualization of lighter structures. The present study proposed ANN-FEM computational framework for the macro-mechanical analysis of multi-oriented Plantain Empty Fruit Bunch Fiber Laminate (PEFBFL) and Plantain Pseudo Stem Fiber Laminate (PPSFL). Control factors were numerically varied using Finite Element Method (FEM) and the resultant FEM models which encapsulated material properties of the laminate was streamlined into Artificial Neural Network (ANN) training scheme. A standard feed-forward backpropagation network was adopted and the ANN model consists of stacking sequence, laminate aspect ratio and fiber orientation as input variables while the selected network outputs variables include average stress and displacement. The laminate constitutive equation was developed which enabled the establishment of laminate load deformation affiliation and equivalent elastic constants. The damage onset for individual lamina was detected by the maximum principal stress theory and the overall laminate strength of 40.12 N/mm^2 was obtained for PEFBFL and 32.16N/mm^2 for PPSFL. On the whole, there was steady reduction in laminates elastic modulus which points to compromised stiffness in material principal axis arising from gradual failure of the plies, this trend continued until the last ply failure occurred in ply 3 and 4 at 90 degrees in tensile mode of transverse direction. Stresses and displacements observed using CLT agree very closely with predictions of ANN.

1. Introduction

Natural fibers have been traditionally utilized over the years to address human needs such as in production of sacks, ropes, bags, rugs, floor covers, carpet backs, binder twines, hats, mats, baskets, stuffing material for upholstery and mattresses due to their low cost, low density, fair specific modulus, high toughness, non-toxic, recyclability and availability compared with synthetic fibers [1; 2]. Additionally, these properties have become the center of attraction for the surge in utilization of natural fibers in reinforcing polymer matrix for application in automotive [3], civil works and transportation sector [4], oil and gas sector [5], wind energy industry [6], housing sector [7], maritime sector [8], power and telecommunication industries [9]. Although, the greater part of the natural fibers such as those extracted from plantain plant are hydrophilic naturally leading to poor interfacial bond with hydrophobic polymer matrix [10], it can still be used successfully as a reinforcement after effective chemical treatment [11].

Continued exploration of post-harvest plantain plant residues in the development of engineering materials such as reinforced composites has been on the increase. Natural fibers extracted from bio wastes offer significant advantage over woody biomass, since they have low micro-fibril angle, small lumen mean, high cellulose content, high crystallinity and relatively longer fibers which gives better control of fiber lay-up and orientation [12; 13; 14]. The use of biodegradable and locally available Plantain Pseudo Stem (PPS) and Empty Fruit Bunch (EFB) fibers from renewable agricultural sources in fabrication of Plantain Empty Fruit Bunch Fiber Reinforced Composite and Plantain Pseudo Stem Fiber Reinforced

* Corresponding author. Tel.: +2348033622498
E-mail address: ce.okafor@unizik.edu.ng

DOI: 10.22075/MACS.2021.20579.1263
Received 2020-06-09; Received in revised form 2020-08-17; Accepted 2021-04-01

Composite have been reported and assessed [15; 16].

Extensive research evidence has thereafter emerged regarding various physical and mechanical properties of plantain fiber reinforced composites [15; 17; 16; 18; 11; 19; 20; 21; 22]; nonetheless, majority of these studies has concentrated on the properties of single plies which consists of unidirectional fiber reinforced lamina. Generally, reinforced composites in which fibers are aligned in one direction would be very weak in the transverse direction; consequently, any small transverse load arising from uneven lateral contraction can initiation crack. There is therefore need to combine some of the best aspects of unidirectional plantain fiber reinforced laminas in order to achieve a more robust material, this is because incorporation of variously oriented plies in one laminate will definitely lead to significant advantages when compared with conventional monolithic materials [23].

The boundless coalescence of ply orientations and stacking sequence obtainable at the design stage of laminates provides the necessary design pliancy to achieve high modulus industrial materials [24]. In this regard, laminated composites can be tailored for directional stiffness properties in longitudinal and transverse directions via combination of axis and off axis laminates. This is essential to guard against catastrophic failure in a way that peradventure any of the layers fail first, the composite can still endure more loads prior to the eventual failure of last ply [25]. Obviously, the failure stress and stiffness properties of plantain fiber reinforced laminates can be acquired through numerical techniques [26; 27]. Basically, the principles of laminated composite material mechanics can be learned at a macro-scale where mechanical behaviour of the laminate and the structure are the primary focal point of investigations [28]. This provides superior initial guess for the designer in terms of average properties of the composite material [29; 30; 31]. Advanced numerical and computational tools have evolved over the years for application in solving diverse composite design problems and skilful utilization of these tools would further diminish the design and improvement time alongside the expense of experimentation expected in the design development phase of laminates.

Rahimi, Hussain, Meon and Mahmud [32] reported that ANSYS software is capable of predicting the failure of composite laminates based on Maximum Stress and Tsai-Wu theories. Saxena and Kirtania [33] used finite element analysis and analytical methods in evaluation of symmetric cross-ply laminated composite plates, authors computational results compared closely with the theoretical results. Other researchers has reported comparable results between finite element and analytical methods for inter-laminar stresses in laminated composite beam [34], first ply failure of laminated composite plates [35], cross-ply laminate of boron/epoxy composite failure under uniformly distributed load [36], failure of inter-ply hybrid laminated composite [37], failure of carbon fiber-reinforced polymer laminated composite thin-walled I-beams [38] and failure of fiber/epoxy composite laminate interface using cohesive multi-scale model [39]. It is necessary to integrate finite element analysis and artificial neural network in order to boost accuracy and speed in design process.

Various macro-mechanical models such as elasticity models [40], plasticity models [41] and nonlinear constitutive model [42] have also been formulated to embody the constitutive affiliations of laminates. Hsuan-Teh and Lung-Shen [42] carried out constitutive modelling of composite laminates under uniaxial compression, authors detected damage onset using Tsai-Wu and the maximum stress criterion. Dimitrienko [43] developed universal models of laminated composites constitutive relations with discrete information on main conjugated stress-strain tensors pairs. Development of a constitutive equation for a novel plantain fiber reinforced laminate is required for establishment of the laminate load deformation affiliation and equivalent elastic constants.

There is also need to relate the externally applied force on plantain fiber reinforced laminate to the resulting deformation of strain stresses at ply level, this will provide the best standing to determine whether any ply has failed using appropriate failure theory. Different failure theories have been used in the literature to evaluate failure initiation in fiber reinforced laminates; Rajanish, Nanjundaradhya, Ramesh and Bhaskar [44] classified them into limit/non-interactive (maximum stress and maximum strain); interactive (TsaiHill and Tsai-Wu) and partially-interactive (Hashin-Rotem and Puck) theories. The validity and criteria for selecting any of these theories is well documented [45; 46; 47]. The non-interactive maximum principal stress criterion was adopted in the present study to account for various ply failure modes inherent in plantain fiber reinforced laminate.

2. Methodology

2.1. Determination of effective ply thickness

The fiber mass fraction M_f is determined from eq. (1) and the ply thickness in terms of mass fraction of fibers is presented in eq. (2).

$$M_f = \frac{\rho_f v_f}{\rho_f v_f + \rho_m(1 - v_f)} \quad (1)$$

$$t = m_{f2}\left[\frac{1}{\rho_f} + \frac{1}{\rho_m}\left(\frac{1 - M_f}{M_f}\right)\right] \quad (2)$$

where ρ_m is the density of matrix while ρ_f and v_f are the density and optimal volume fraction (50%) of fiber respectively. Properties and characteristics of the plantain fiber reinforcement–polyester matrix with detailed implementation of Archimedes principle has been reported elsewhere [15; 18] and by knowing the density of polyester resin as 1200kg/m^3, the ply thickness from eq. (2) and specific mass of fiber m_{f2} is presented in Table 1.

The individual layers of laminate composites are held together by matrix to form a plate. The layers of the laminate composites referred in the present study are of thesame constituent materials having different reinforcing pattern. The matrix and fiber part of the laminate composite are respectively polyester and plantain fiber with properties described in Tables 2 and 3. Obviously, the analysis of laminate depends on the properties of individual layers and the detailed mechanical properties of single layer of Plantain Empty Fruit Bunch Fiber Reinforced Composite (PEFBFC) and Plantain Pseudo Stem Fiber Reinforced Composite (PPSFC) have been reported by [16].

2.2. Design of experiment and Finite Element modeling

The classical Central Composite Design (CCD) method was used to determine the number of numerical experiments to be evaluated. CCD is a useful design of experiment (DOE) template which minimizes the required number of iterations for full material assessment. It involves varying the stacking sequence from (30/0/90)s to (30/45/90)s, laminate aspect ratio from 1.31 to 0.79 and fiber orientation from 30^0 to 90^0 as shown in Fig. 1. This control factor arrengement gave a total of 26 experimental runs.

The Finite Element Analysis was conducted in ANSYS Parametric Design Language (APDL). A 3D 4-node shell 181 element with six degrees of freedom was used in creating the model following the symmetry of layer code shown in Fig. 1a. According to Abhishek [35], SHELL181 is useful in evaluation of thin to moderately-thick shell structures. The material model was assigned to structural linear elastic orthotropic behaviour and then the shell section was modified to conform to fiber angle orientations and lay-up.

Table 1: Plantain fiber ply parameters determined by application of Archimedes principle

FIBER SOURCE	m_{f2}(g)	v_{f2}(mm^3)	Density kg/m^3	Ply Thickness (mm)
PEFB fiber	20.397	53364.8	381.966	0.108
PSTEM fiber	20.670	58364.8	354.151	0.228

Table 2: Mechanical properties of single layer plantain fibers reinforced polyester composites [16]

Composites	Properties								
	S_{u1} (MPa)	S_{u2} (MPa)	S_y (MPa)	E_1 (MPa)	E_2 (MPa)	E (MPa)	v_{12}	τ_{max} (MPa)	G12 (MPa)
PEFBFC	410.15	37.3397	33.69	14922	7030.962	9990.10	0.38	19.3100	3622.99
PPSFC	288.10	33.1330	29.24	13027.5	6817.175	9146.305	0.29	15.5700	3332.84

Note: S_{u1}, S_{u2} are tensile strengths in the longitudinal and transverse directions respectively.

Table 3: Mechanical properties of plantain fibers and polyester resin [16]

Property	Polyester resin
Young modulus (MPa)	2000 – 4500
Tensile strength (MPa)	40 - 9 0
Compressive strength (MPa)	90 -250
Tensile elongation at break (%)	2
Water absorption 24h at 20 °C	0.1 - 0.3
Flexural modulus (GPa)	11.0
Poisson's ratio.	0.37 – 0.38
	Plantain Pseudo Stem Fibers
Young modulus (MPa)	23555
UTS (MPa)	536.2
Strain (%)	2.37
	Plantain Empty fruit bunch Fibers
Young modulus (MPa)	27344
UTS (MPa)	780.3
Strain (%)	2.68

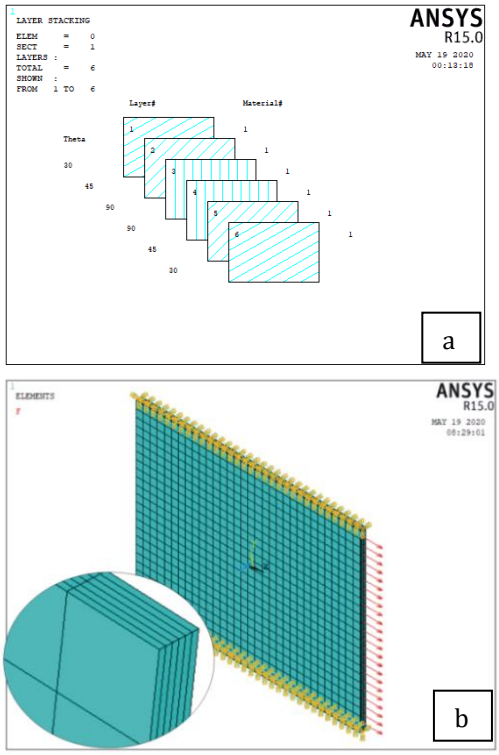

Fig. 1: (a) Stacking sequence and (b) Boundary Condition for PEFBFL (Nodes = 825, Elements = 768)

Each layer thickness corresponds to the ply thickness as specified in Table 1, finite element model was created using rectangular cross section and the meshing was done for the entire laminate at a time. In the post-processing phase, results of laminate stresses in x direction and deformation are viewed and plotted at nodes as shown in Fig. 2.

The data acquired were fitted to the empirical polynomial regression model of eq. (3).

$$Y = \beta_0 + \sum_{i=1}^{k} \beta_i x_i + \sum_{i=1}^{k} \beta_{ii} x_i^2 + \sum_{i=1}^{k-1} \sum_{j}^{k} \beta_{ij} x_i x_j + \varepsilon \quad (3)$$

where Y is responses (stress and displacement); β_0, β_i (i = 1, 2,.....k) and β_{ij} (i = 1, 2,...k; j = 1, 2,...k) are the model coefficients; x_i and x_j are the coded independent variables. Also, the adequacy of the model was checked using the coefficient of determination (R^2).

2.3. Artificial Neural Network training scheme

The Neural Network model was trained using the raw numerical dataset obtained from the finite element simulation. The weighted sum of inputs arriving at each neuron was passed through an activation function to generate an output signal. A total of 17 (65.4%) of experimental results was used to train the network, 5 (19.2%) of the experimental result was used to validate the training while the remaining 4 (15.4%) was used for testing. In order to reduce the deviations of response predictions, a trial and error method was utilised to establish the suitable number of neurons required in the hidden layer, this was achieved by repeating the training cycle at varying number of neurons in the hidden layer. The Multi-layer perceptron which was trained with back-propagation algorithm has three input neurons representing the design independent variables (stacking sequence, laminate aspect ratio and fiber orientation), a single hidden layer of ten neurons and an output layer consisting of two neurons representing the stress and displacement as shown in Fig. 4. The network performance was assessed using Mean Square Error (MSE) and coefficient of determination (R^2). Error minimization was achieved by Levenberge–Marquardt (LM) method. The Levenberg-Marquardt algorithm uses an approximation to the Hessian Matrix in a Newton-like update shown in Eq. (4).

$$x_{k+1} = x_k \pm [J^T J + \mu I]^{-1} J^T e \quad (4)$$

where J = Jacobian matrix containing first derivatives of the network errors, e = vector of network errors. At $\mu = 0$, eq. (4) becomes the regular Newton's method using an approximate Hessian matrix, however at $\mu \gg 0$, eq. (4) becomes gradient descent with a small step size. The mean sum of squares of the network errors was captured using Eq. (5).

$$f = MSE = \frac{1}{n}\sum_{i=1}^{n}(e_i)^2 \quad (5)$$

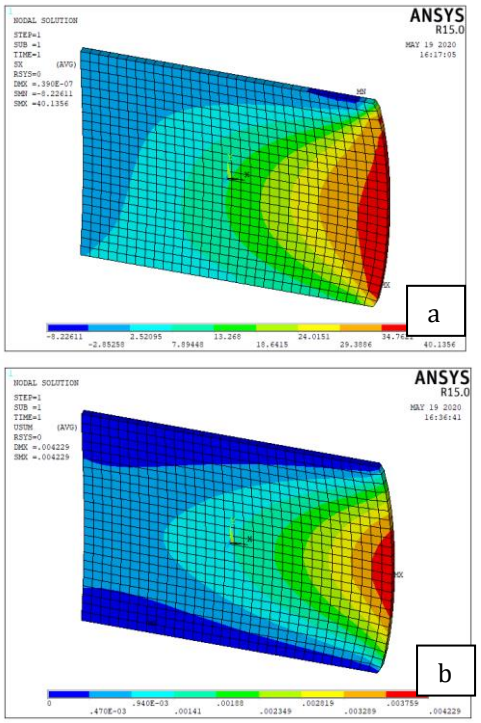

Fig. 2: (a)Laminate Stresses and (b) Displacement in x direction for PEFBFL

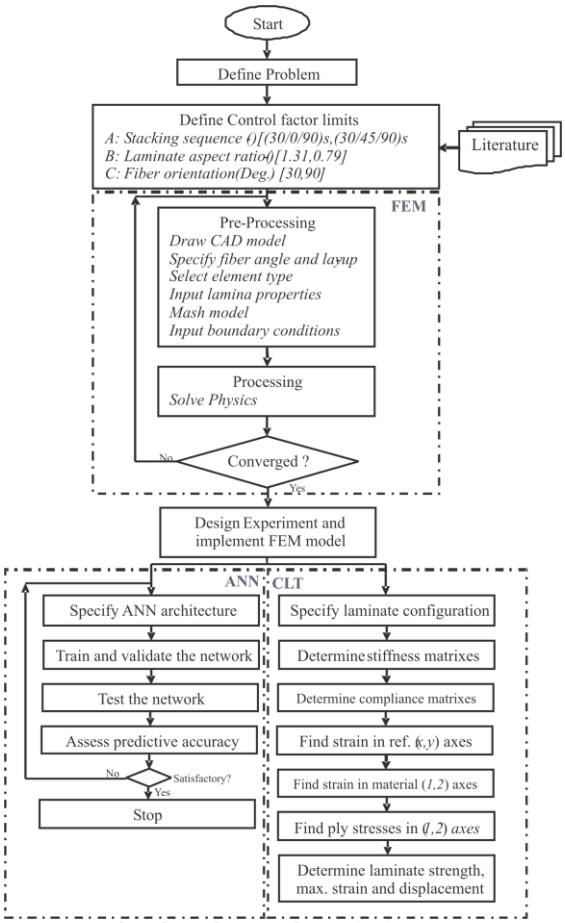

Fig. 3: Flowchart showing the graft of ANN-FEM technique

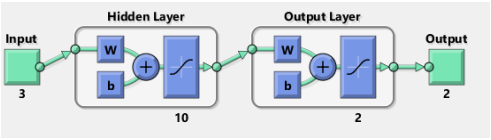

Fig. 4: Artificial neural network with 3 input variables, 1 hidden layer of 10 neurons and 2 output variables.

2.4. Formulation of laminate stiffness framework

Following classical laminate theory [48; 49; 29], the variation of direct strain in x and y is given in eq. (6). Classical Laminate Theory (CLT) is a predictive means used in the analysis of laminate behaviour based on its stacking sequence and material properties. The theory assumed that each layer of the laminate is both quasihomogeneous and orthotropic; the thickness of the plate is much smaller than any of its characteristic dimension; the displacements arising from mechanical loading is small compared with thickness of the plate; the in-plane strains are small compared with unity; transverse shear and normal strain are negligible; no warping exist; each ply obeys Hooke's Law and the plate thickness is constant throughout the laminate. Eqs. 6-20 provides the mathematical background for application of CLT.

$$\left.\begin{aligned} e_x &= \frac{du_0}{dx} - z\frac{d^2w_0}{dx^2} = e_x^0 - zk_x \\ e_y &= \frac{dv_0}{dy} - z\frac{d^2w_0}{dy^2} = e_y^0 - zk_y \end{aligned}\right\} \quad (6)$$

and shear strain in x-y plane reads:

$$e_{xy} = \frac{du_0}{dy} + \frac{dv_0}{dx} - z\frac{d^2w_0}{dy^2} = e_{yx}^0 - zk_{xy} \quad (7)$$

Combining eqs. 6 -7 in a matrix form gives:

$$\begin{bmatrix} e_x \\ e_y \\ e_{xy} \end{bmatrix} = \begin{bmatrix} e_x^0 \\ e_y^0 \\ e_{yx}^0 \end{bmatrix} - z\begin{bmatrix} k_x \\ k_y \\ k_{xy} \end{bmatrix} \quad (8)$$

Integrating in-plane force intensities and moment over the thickness of ply p in x,y and x-y-directions reads:

$$[N_x]_p = \int_{z_{p-1}}^{z_p} \sigma_x dz\,; [M_x]_p = -\int_{z_{p-1}}^{z_p} \sigma_x z dz \quad (9)$$

$$[N_y]_p = \int_{z_{p-1}}^{z_p} \sigma_y dz\,; [M_y]_p = -\int_{z_{p-1}}^{z_p} \sigma_y z dz \quad (10)$$

$$[N_{xy}]_p = \int_{z_{p-1}}^{z_p} \sigma_{xy} dz\,; [M_{xy}]_p = -\int_{z_{p-1}}^{z_p} \sigma_{xy} z dz \quad (11)$$

The knowledge of σ_x, σ_y and σ_{xy} on the plies is necessary for complete evaluation of eqs. (9 – 11). Considering two possible loading conditions of longitudinal (direction 1) and transverse (direction 2) in the matrix, the resulting direct strains from Hooks law are respectively $e_1 = \frac{-v_{21}\sigma_1}{E_1}$ and $e_2 = \frac{-v_{12}\sigma_1}{E_1}$ where v_{12} = major Poisson's ratio and v_{21} = minor Poisson's ratio. Hence the application of both direct stresses σ_1 and σ_2 will yield corresponding strains as follows:

$$e_1 = \frac{\sigma_1}{E_1} - \frac{v_{21}\sigma_2}{E_2}, e_2 = \frac{\sigma_2}{E_2} - \frac{v_{12}\sigma_1}{E_1} \quad (12)$$

And the stress-strain relationship for an orthotropic ply can be expressed as:

$$\begin{bmatrix} \sigma_x \\ \sigma_y \\ \tau_{xy} \end{bmatrix} = \begin{bmatrix} \bar{Q}_{11} & \bar{Q}_{12} & \bar{Q}_{13} \\ \bar{Q}_{12} & \bar{Q}_{22} & \bar{Q}_{23} \\ \bar{Q}_{13} & \bar{Q}_{23} & \bar{Q}_{33} \end{bmatrix} \begin{bmatrix} e_x \\ e_y \\ e_{xy} \end{bmatrix} \quad (13)$$

where

$$\bar{Q}_{11} = cos^4\theta Q_{11} + sin^4\theta Q_{22} + 2cos^2\theta sin^2\theta Q_{12} + 4cos^2\theta sin^2\theta Q_{33}$$

$$\bar{Q}_{22} = sin^4\theta Q_{11} + cos^4\theta Q_{22} + 2cos^2\theta sin^2\theta Q_{12} + 4cos^2\theta sin^2\theta Q_{33}$$

$$\bar{Q}_{33} = cos^2\theta sin^2\theta Q_{11} + cos^2\theta sin^2\theta Q_{22} - 2cos^2\theta sin^2\theta Q_{12} + (cos^2\theta - sin^2\theta)^2 Q_{33}$$

$$\bar{Q}_{12} = cos^2\theta sin^2\theta Q_{11} + cos^2\theta sin^2\theta Q_{22} + (cos^4\theta + sin^4\theta)Q_{12} - 4cos^2\theta sin^2\theta Q_{33}$$

$$\bar{Q}_{13} = cos^3\theta sin\theta Q_{11} - cos\theta sin^3\theta Q_{22} + (cos\theta sin^3\theta - cos^3\theta sin\theta)Q_{12} + 2(cos\theta sin^3\theta - cos^3\theta sin\theta)Q_{33}$$

$$\bar{Q}_{23} = cos\theta sin^3\theta Q_{11} - cos^3\theta sin\theta Q_{22} + (cos^3\theta sin\theta - cos\theta sin^3\theta)Q_{12} + 2(cos^3\theta sin\theta - cos\theta sin^3\theta)Q_{33}$$

Combining eq. (13) with eq. (8), we have:

$$\begin{bmatrix} N_x \\ N_y \\ N_{xy} \end{bmatrix}_p = \begin{bmatrix} A_{11} & A_{12} & A_{13} \\ A_{12} & A_{22} & A_{23} \\ A_{13} & A_{23} & A_{33} \end{bmatrix} \begin{bmatrix} e_x^0 \\ e_y^0 \\ e_{yx}^0 \end{bmatrix} + \begin{bmatrix} B_{11} & B_{12} & B_{13} \\ B_{12} & B_{22} & B_{23} \\ B_{13} & B_{23} & B_{33} \end{bmatrix} \begin{bmatrix} k_x \\ k_y \\ k_{xy} \end{bmatrix} \quad (14)$$

Eq. (14) describes the association between the applied force (N) and the resulting midplane laminate deformations. While the extensional and coupling stiffnessis presented in eqs. (15) and (16) respectively.

$$A_{ij} = \sum_{p=1}^{n} (z_p - z_{p-1}) \left(\bar{Q}_{ij}\right)_p = \sum_{p=1}^{n} (t_p) \left(\bar{Q}_{ij}\right)_p \quad (15)$$

$$B_{ij} = \sum_{p=1}^{n} -\left(\frac{z_p^2 - z_{p-1}^2}{2}\right) \left(\bar{Q}_{ij}\right)_p = \sum_{p=1}^{n} -(t_p \bar{z}_p) \left(\bar{Q}_{ij}\right)_p \quad (16)$$

In similar consideration for moment about specific axis for ply 1to n in Fig. 1 gives:

$$\begin{bmatrix} M_x \\ M_y \\ M_{xy} \end{bmatrix}_p = \begin{bmatrix} B_{11} & B_{12} & B_{13} \\ B_{12} & B_{22} & B_{23} \\ B_{13} & B_{23} & B_{33} \end{bmatrix} \begin{bmatrix} e_x^0 \\ e_y^0 \\ e_{yx}^0 \end{bmatrix} + \begin{bmatrix} D_{11} & D_{12} & D_{13} \\ D_{12} & D_{22} & D_{23} \\ D_{13} & D_{23} & D_{33} \end{bmatrix} \begin{bmatrix} k_x \\ k_y \\ k_{xy} \end{bmatrix} \quad (17)$$

Eq. (17) gives the bending stiffness term (D_{ij}) which depends on transformed reduced stiffness term $\left(\bar{Q}_{ij}\right)$ and the ply cordinate terms.

$$D_{ij} = \sum_{p=1}^{n} \left(\frac{z_p^3 - z_{p-1}^3}{3}\right) \left(\bar{Q}_{ij}\right)_p = \sum_{p=1}^{n} \left(t_p \bar{z}_p^2 + \frac{t_p^2}{12}\right) \left(\bar{Q}_{ij}\right)_p \quad (18)$$

Inversion of the laminate stiffness terms in eq. (13) yields the required transformed reduced compliance terms a_{ij}, so considering a fully populated extensional stiffness matrices (strain component of eq. (14)

$$a = \begin{bmatrix} \frac{(A_{22}A_{33} - A_{23}^2)}{AA} & \frac{(A_{13}A_{23} - A_{12}A_{33})}{AA} & \frac{(A_{12}A_{23} - A_{22}A_{13})}{AA} \\ \frac{(A_{13}A_{23} - A_{12}A_{33})}{AA} & \frac{(A_{11}A_{33} - A_{13}^2)}{AA} & \frac{(A_{12}A_{13} - A_{11}A_{23})}{AA} \\ \frac{(A_{12}A_{23} - A_{22}A_{13})}{AA} & \frac{(A_{12}A_{13} - A_{11}A_{23})}{AA} & \frac{(A_{11}A_{22} - A_{12}^2)}{AA} \end{bmatrix} \quad (19)$$

Where $AA = A_{11}A_{22}A_{33} + 2A_{12}A_{23}A_{13} - A_{22}A_{13}^2 - A_{33}A_{12}^2 - A_{11}A_{23}^2$

Considering a fully populated bending stiffness matrices (k component of eq. 14)

$$d = \begin{bmatrix} \frac{(D_{22}D_{33} - D_{23}^2)}{DD} & \frac{(D_{13}D_{23} - D_{12}D_{33})}{DD} & \frac{(D_{12}D_{23} - D_{22}D_{13})}{DD} \\ \frac{(D_{13}D_{23} - D_{12}D_{33})}{DD} & \frac{(D_{11}D_{33} - D_{13}^2)}{DD} & \frac{(D_{12}D_{13} - D_{11}D_{23})}{DD} \\ \frac{(D_{12}D_{23} - D_{22}D_{13})}{DD} & \frac{(D_{12}D_{13} - D_{11}D_{23})}{DD} & \frac{(D_{11}D_{22} - D_{12}^2)}{DD} \end{bmatrix} \quad (20)$$

Where$DD = D_{11}D_{22}D_{33} + 2D_{12}D_{23}D_{13} - D_{22}D_{13}^2 - D_{33}D_{12}^2 - D_{11}D_{23}^2$

3. Results and discussions

3.1. CCD optimum conditions

The optimization exercise for stress and displacement was conducted utilizing the flexibility of the Design Expert optimization tool function. Eq. (3) was solved for the best solutions. A usual approach which involves selecting the best solution was adopted and the chosen optimal solutions gave stacking sequence = (30/45/90)s, laminate aspect ratio = 1.31, fiber orientation = 90^0 and desirability = 1. The laminate with optimum characteristics was further analyzed by applying the Classical Laminate Theory along the thickness of specified fiber source.

3.2. ANN training evaluation and performance

The training record was used to plot the performance progress. The Mean Square Error of the trained network for PEFBFL strength prediction was 0.46, having a regression coefficient of 0.99 while the network for PEFBFL displacement prediction has Mean Square Error of 4.55442E-09 and regression coefficient of 0.93 (Figs. 5 & 6). Similarly, The Mean Square Error of the trained network for PPSFL strength prediction is 0.6557, having a regression

coefficient of 0.96 while the network for PEFBFL displacement prediction has Mean Square Error of 1.25768E-09 and regression coefficient of 0.94 (Figs. 7 & 8). In all, the training data indicates a good fit and the validation results also show reasonably high R^2 values that are close to 1. The regression coefficient measures the correlation between the predicted responses (outputs) and the experimental responses (targets).

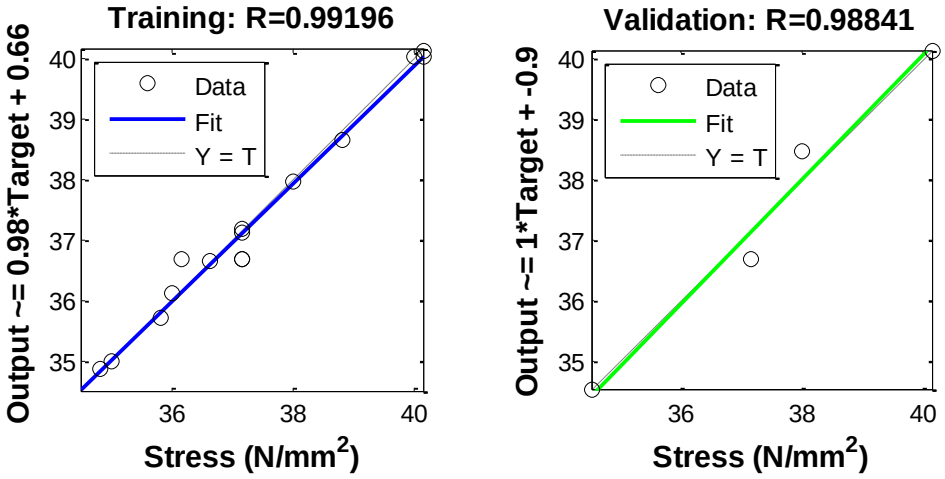

Fig. 5: (a) Actual value of PEFBFL stress versus predicted (b) Regression plot for validation

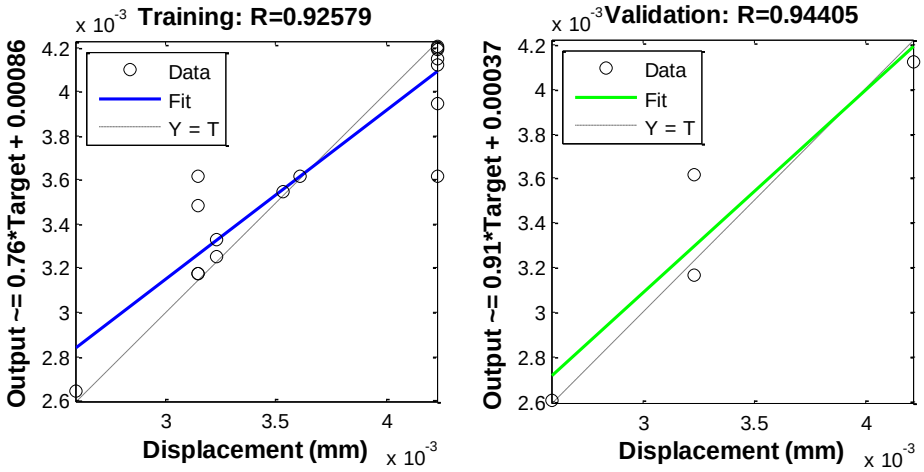

Fig. 6: (a) Actual value of PEFBFL displacement versus predicted (b) Regression plot forvalidation

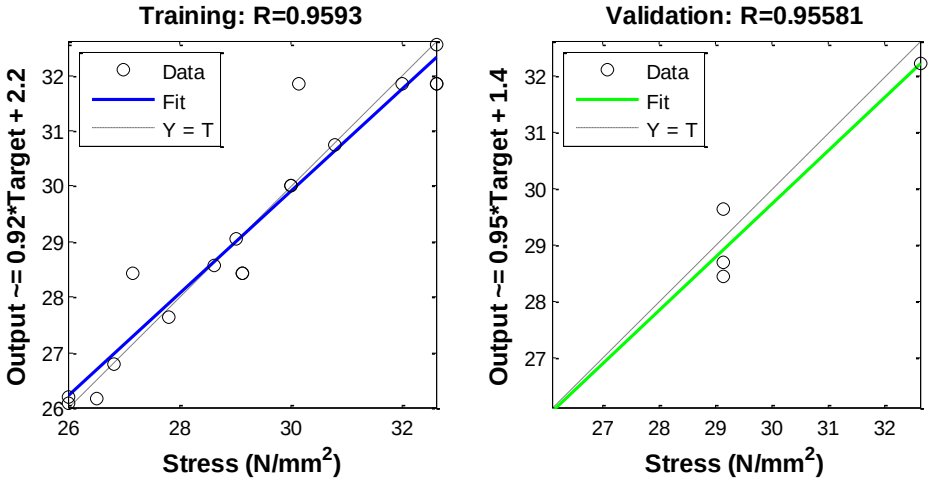

Fig. 7: (a) Actual value of PPSFL stress versus predicted (b) Regression plot for validation

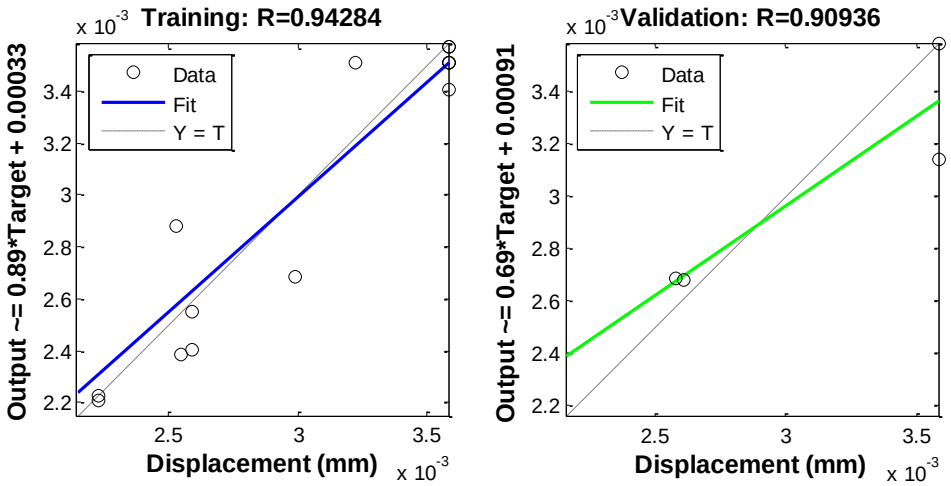

Fig. 8: (a) Actual PPSFL value of displacement versus predicted (b) Regression plot for validation

3.3. Overall reduced stiffness terms

The optimal set of plantain fiber reinforced laminate with thickness (t) which is composed of six stacked plies in the order $(30/45/90)_s$ is represented in Fig. 9.

Minor Poisson's Ratio is the strain resulting from stress in the axial direction. The minor Poisson's ratio v_{21} for single layer plantain fibers reinforced polyester composites using eq. (12) and relevant data in Table 1 is found as:

$$v_{21,\text{PEFBFC}} = \frac{E_2 v_{12}}{E_1} = \frac{7030.962 * 0.38}{14{,}922} = 0.179$$

$$v_{21,\text{PPSFC}} = \frac{E_2 v_{12}}{E_1} = \frac{6817.175 * 0.29}{13027.5} = 0.152$$

Similarly, the ply reduced stiffness matrix (Q) for a single layer of PEFBFC (N/mm²) and single layer PPSFC (N/mm²) is also evaluated and presented in eq. (21) For PEFBFC and For PPSFC in eq. (22).

$$Q_{\text{PEFBFC}} = \begin{Bmatrix} 16011.07 & 2865.98 & 0 \\ 2865.98 & 7544.113 & 0 \\ 0 & 0 & 3622.99 \end{Bmatrix} \quad (21)$$

$$Q_{\text{PPSFC}} = \begin{Bmatrix} 13628.23 & 2071.49 & 0 \\ 2071.49 & 7131.53 & 0 \\ 0 & 0 & 3332.835 \end{Bmatrix} \quad (22)$$

Hence the transformed reduced stiffness term for the multi-oriented plantain fiber/polyester laminate described in Fig. 10 is obtained from eq. (13) and presented in Table 4 for PEFBFL and Table 5 for PPSFL.

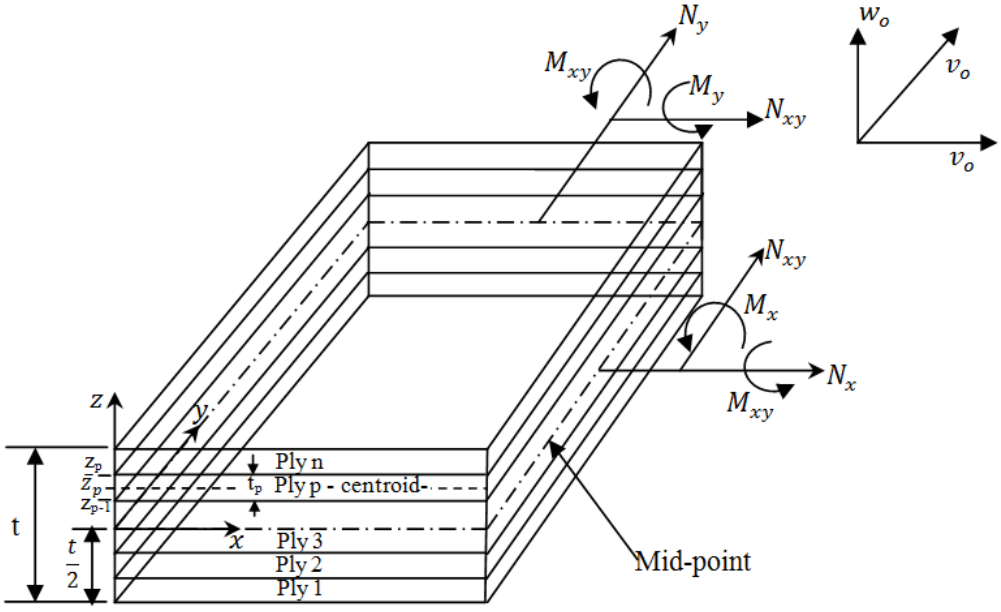

Fig. 9: Elements of the laminate showing point force and moment strengths

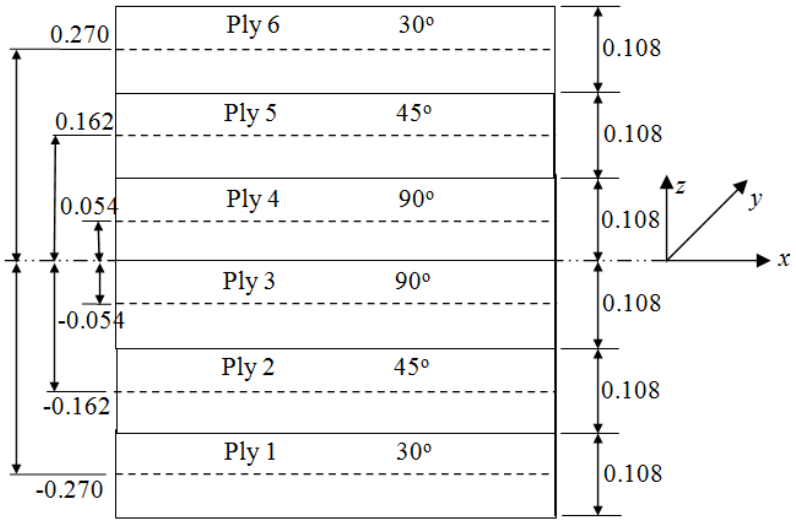

Fig. 10: Six layer PEFB fiber symmetric laminate code (mm)

Table 4: $\bar{Q}_{ij}$ values (N/mm^2) for PEFBFL (30/45/90)s

Ply	Fiber Orientation (Degree)	$\bar{Q}_{11}$	$\bar{Q}_{22}$	$\bar{Q}_{33}$	$\bar{Q}_{12}$	$\bar{Q}_{13}$	$\bar{Q}_{23}$
1	30	13269.72	9036.24	4247.60	3490.59	2193.77	1472.53
2	45	10944.78	10944.78	4455.81	3699.00	2116.74	2117.00
3	90	7544.11	16011.07	3622.99	2866.00	0.00	0.00
4	90	7544.11	16011.07	3622.99	2866.00	0.00	0.00
5	45	10944.78	10944.78	4455.81	3699.00	2116.74	2117.00
6	30	13269.72	9036.24	4247.60	3491.00	2193.77	1472.53

Table 5: $\bar{Q}_{ij}$ values (N/mm^2) for PPSFL $(30/45/90)_s$

Ply	Fiber Orientation (Degree)	$\bar{Q}_{11}$	$\bar{Q}_{22}$	$\bar{Q}_{33}$	$\bar{Q}_{12}$	$\bar{Q}_{13}$	$\bar{Q}_{23}$
1	30	11388.02	8139.69	3948.85	2687.50	1762.22	1050.92
2	45	9558.52	9558.52	4154.19	2892.84	1624.17	1624.17
3	90	7131.53	13628.2	3332.84	2071.49	0	0
4	90	7131.53	13628.2	3332.84	2071.49	0	0
5	45	9558.52	9558.52	4154.19	2892.84	1624.17	1624.17
6	30	11388.02	8139.69	3948.85	2687.5	1762.22	1050.92

Since the laminate in this study is symmetric, the coupling B_{ij} described in eq. (16) tends to zero while the extensional A_{ij} and bending D_{ij} stiffness terms are computed using the ply thickness and centroidal values described in Fig. 10 and tabulations in Table 6 for PEFBFL and in Table 7 for PPSFL.

The extensional stiffness A_{ij}(N/mm) and bending $D_{ij}(N-mm)$stiffness as defined in eqs. (15) and (18) are computed using plies 1, 2 and 3 in turn doubling the result in consideration of ply symmetry to get total laminate extensional and bending stiffness written in matrix form in eq. (23) to (26) for PEFBFL and PPSFL.

$$A_{\text{PEFBFL}} = \begin{bmatrix} 6859.859 & 2172.008 & 931.0699 \\ 2172.008 & 7774.291 & 775.3385 \\ 931.0699 & 775.3385 & 2662.502 \end{bmatrix} \quad (23)$$

$$D_{\text{PEFBFL}} = \begin{bmatrix} 282.41249 & 79.84915 & 47.448143 \\ 79.84915 & 221.97223 & 35.941324 \\ 47.448143 & 35.941324 & 97.012995 \end{bmatrix} \quad (24)$$

$$A_{\text{PPSFL}} = \begin{bmatrix} 12803.6 & 3489.235 & 1544.196 \\ 3489.235 & 14284.84 & 1219.839 \\ 1544.196 & 1219.839 & 5214.762 \end{bmatrix} \quad (25)$$

$$D_{\text{PPSFL}} = \begin{bmatrix} 2294.7227 & 579.84773 & 354.39678 \\ 579.84773 & 1858.3847 & 247.60829 \\ 354.39678 & 247.60829 & 848.94709 \end{bmatrix} \quad (26)$$

Evaluation of eqs. (19) and (20) gives the transformed reduced compliance $a_{ij}\left(\frac{1}{\text{N/mm}}\right)$ and bending stiffness $d_{ij}\left(\frac{1}{\text{N-mm}}\right)$ matrices for PEFBFL and PPSFL as shown in eq. (27) to (30).

$$a_{\text{PEFBFL}} = \begin{bmatrix} 0.000165 & -4.2\text{E}-05 & -4.6\text{E}-05 \\ -4.2\text{E}-05 & 0.000143 & -2.7\text{E}-05 \\ -4.6\text{E}-05 & -2.7\text{E}-05 & 0.000399 \end{bmatrix} \quad (27)$$

$$d_{\text{PEFBFL}} = \begin{bmatrix} 0.0041559 & -0.00124 & -0.001573 \\ -0.00124 & 0.0051627 & -0.001306 \\ -0.001573 & -0.001306 & 0.0115612 \end{bmatrix} \quad (28)$$

$$a_{\text{PPSFL}} = \begin{bmatrix} 8.59\text{E}-05 & -1.9\text{E}-05 & -2.1\text{E}-05 \\ -1.9\text{E}-05 & 7.57\text{E}-05 & -1.2\text{E}-05 \\ -2.1\text{E}-05 & -1.2\text{E}-05 & 0.000201 \end{bmatrix} \quad (29)$$

$$d_{\text{PPSFL}} = \begin{bmatrix} 0.0004951 & -0.000132 & -0.000168 \\ -0.000132 & 0.0005951 & -0.000118 \\ -0.000168 & -0.000118 & 0.0012827 \end{bmatrix} \quad (30)$$

The laminate equivalent elastic constants are therefore computed for membrane and bending modes using appropriate expressions in Table 8.

3.4. Macroscopic assessment of ply failure based on Maximum Principal Stress Theory

Ply strength analysis was performed using Maximum Principal Stress Theory, the use of this noninteractive failure criterion was justified because of the need to ascertain probable laminar mode of failure. The load required to cause the first ply failure was obtained from the strength ratio of the plies. The maximum strength ratio was subsequently used to calculate the load factor and the load intensity required to cause the first ply failure.

Table 6: Ordinate values for PEFBFL $(30/45/90)_s$

Ply	Fiber Orientation (Degree)	t_p (mm)	$\bar{z}_p$ (mm)	$\left(t_p\bar{z}_p^2+\frac{t_p^2}{12}\right)$ (mm)
1	30	0.108	-0.27	0.00798
2	45	0.108	-0.162	0.00294
3	90	0.108	-0.054	0.00042
4	90	0.108	0.054	0.00042
5	45	0.108	0.162	0.00294
6	30	0.108	0.27	0.00798

Table 7: Ordinate values for PPSFL $(30/45/90)_s$

Ply	Fiber Orientation (Degree)	t_p (mm)	$\bar{z}_p$ (mm)	$\left(t_p\bar{z}_p^2+\frac{t_p^2}{12}\right)$ (mm)
1	30	0.228	-0.57	0.07506
2	45	0.228	-0.342	0.02766
3	90	0.228	-0.114	0.00395
4	90	0.228	0.114	0.00395
5	45	0.228	0.342	0.02766
6	30	0.228	0.57	0.07506

Table 8: Equivalent elastic constants of laminates

Elastic constant	Membrane mode			Bending mode		
	Source	Result		Source	Result	
		PEFBFL	PPSFL		PEFBFL	PPSFL
$E_x =$	$\frac{1}{t\left(\frac{A_{22}A_{33}-A_{23}^2}{AA}\right)}$	93450.41	8514.19	$\frac{12}{t^3\left(\frac{D_{22}D_{33}-D_{23}^2}{DD}\right)}$	10611873.8	9466.81
$E_y =$	$\frac{1}{t\left(\frac{A_{11}A_{33}-A_{13}^2}{AA}\right)}$	107955.6	9654.24	$\frac{12}{t^3\left(\frac{D_{11}D_{33}-D_{13}^2}{DD}\right)}$	8542388.10	7876.59
$G_{xy} =$	$\frac{1}{t\left(\frac{A_{11}A_{22}-A_{12}^2}{AA}\right)}$	38634.96	3640.82	$\frac{12}{t^3\left(\frac{D_{11}D_{22}-D_{12}^2}{DD}\right)}$	3814649.15	3654.32
$v_{xy} =$	$-\frac{\left(\frac{A_{13}A_{23}-A_{12}A_{33}}{AA}\right)}{\left(\frac{A_{22}A_{33}-A_{23}^2}{AA}\right)}$	0.25	0.22	$-\frac{\left(\frac{D_{13}D_{23}-D_{12}D_{33}}{DD}\right)}{\left(\frac{D_{22}D_{33}-D_{23}^2}{DD}\right)}$	0.30	0.27
$y_{yx} =$	$-\frac{\left(\frac{A_{13}A_{23}-A_{12}A_{33}}{AA}\right)}{\left(\frac{A_{11}A_{33}-A_{13}^2}{AA}\right)}$	0.29	0.25	$-\frac{\left(\frac{D_{13}D_{23}-D_{12}D_{33}}{DD}\right)}{\left(\frac{D_{11}D_{33}-D_{13}^2}{DD}\right)}$	0.24	0.22
$m_x =$	$-\frac{\left(\frac{A_{12}A_{23}-A_{22}A_{13}}{AA}\right)}{\left(\frac{A_{22}A_{33}-A_{23}^2}{AA}\right)}$	0.28	0.24	$-\frac{\left(\frac{D_{12}D_{23}-D_{22}D_{13}}{DD}\right)}{\left(\frac{D_{22}D_{33}-D_{23}^2}{DD}\right)}$	0.38	0.34
$m_y =$	$-\frac{\left(\frac{A_{12}A_{13}-A_{11}A_{23}}{AA}\right)}{\left(\frac{A_{11}A_{33}-A_{13}^2}{AA}\right)}$	0.19	0.16	$-\frac{\left(\frac{D_{12}D_{13}-D_{11}D_{23}}{DD}\right)}{\left(\frac{D_{11}D_{33}-D_{13}^2}{DD}\right)}$	0.25	0.20

Notably, the load factor is inversely proportional to the strength ratio only for Maximum Principal Stress Theory. However, for Tsai-Hill failure criterion, the load factor is inversely proportional to the square root of strength ratio. For Hoffman criterion and Tsai-Wu criterion, the relationship between load factor and strength ratio has combination of quadratic and linear functions. Hence for initial design development phase of laminates, Maximum Principal Stress Theory is adjudged valid.

3.4.1. First-ply-failure analysis:

Considering only membrane load, a partially populated compliance matrices is obtained from eq. (19) and by applying theordinate values for PEFBFL ply laminate $(30/45/90)_s$ in Fig. 6:

$L_{11} = 2\{(0.108 \times 13269.72)_{Ply\ 1} + (0.108 \times 10944.78)_{Ply\ 2} + (0.108 \times 7544.11)_{Ply\ 3}\} = 6859.86$

$L_{22} = 2\{(0.108 \times 9036.24)_{Ply\ 1} + (0.108 \times 10944.78)_{Ply\ 2} + (0.108 \times 16011.07)_{Ply\ 3}\} = 7774.292$

$L_{33} = 2\{(0.108 \times 4247.60)_{Ply\ 1} + (0.108 \times 4455.81)_{Ply\ 2} + (0.108 \times 3622.99)_{Ply\ 3}\} = 2662.503$

$L_{12} = 2\{(0.108 \times 3490.59)_{Ply\ 1} + (0.108 \times 3698.8)_{Ply\ 2} + (0.108 \times 2865.98)_{Ply\ 3}\} = 2791.012$

$$L = \begin{bmatrix} L_{11} & L_{12} & 0 \\ L_{12} & L_{22} & 0 \\ 0 & 0 & L_{33} \end{bmatrix} = \begin{bmatrix} 6859.86 & 2791.012 & 0 \\ 2791.012 & 7774.292 & 0 \\ 0 & 0 & 2662.503 \end{bmatrix}$$

$$l = \begin{bmatrix} \frac{L_{22}}{LL} & \frac{-L_{12}}{LL} & 0 \\ \frac{-L_{12}}{LL} & \frac{L_{11}}{LL} & 0 \\ 0 & 0 & \frac{1}{L_{33}} \end{bmatrix} = \begin{bmatrix} 0.0001599 & -4.47\text{E}-05 & 0 \\ -4.47\text{E}-05 & 0.0001599 & 0 \\ 0 & 0 & 0.000376 \end{bmatrix}$$

And a membrane equivalent Young's modulus (E_x) in the direction of the applied load is

$$E_x = \frac{1}{t\left(\frac{L_{22}}{LL}\right)} = \frac{1}{0.648\left(\frac{6859.86}{48613136.28}\right)} = 9649.789\ (\text{N/mm}^2)$$

where t is the total thickness of the laminate (t_p× number of layers) and $LL = L_{11}L_{22} - L_{12}^2$. An axial load of 476N is applied at first instance to the 25×19.05 (LW) rectangular section of Fig. 1, the force intensity N_x is the axial force per unit width of the section ($N_x = 476/19.05 = 25N/mm$ as $N_y = 0$ and $N_{xy} = 0$). Then the laminate mid-plane deformations strains e_x^o, e_y^o, e_{xy}^o at the laminate reference axes are calculated for each ply using eq. (31).

$$\begin{Bmatrix} e_x^0 \\ e_y^0 \\ e_{yx}^0 \end{Bmatrix} = \begin{Bmatrix} \frac{L_{22}}{LL} & \frac{-L_{12}}{LL} & 0 \\ \frac{-L_{12}}{LL} & \frac{L_{11}}{LL} & 0 \\ 0 & 0 & \frac{1}{L_{33}} \end{Bmatrix} \begin{Bmatrix} N_x \\ N_y \\ N_{xy} \end{Bmatrix} \quad (31)$$

Or

$$\begin{Bmatrix} e_x^0 \\ e_y^0 \\ e_{yx}^0 \end{Bmatrix} = \begin{Bmatrix} 0.0001599 & -4.47\text{E}-05 & 0 \\ -4.47\text{E}-05 & 0.0001599 & 0 \\ 0 & 0 & 0.000376 \end{Bmatrix} \begin{Bmatrix} 25 \\ 0 \\ 0 \end{Bmatrix}$$

$$\begin{Bmatrix} e_x^0 \\ e_y^0 \\ e_{yx}^0 \end{Bmatrix} = \begin{Bmatrix} 0.003998 \\ -0.001117 \\ 0 \end{Bmatrix} \quad (32)$$

3.3.1.1.*Computation of PEFBFL ply strain in material axes:*

Eq. (32) is the constant strain distribution through the laminate thickness in all the three symmetric plies. However, the ply strain in the material reference axes is related to the material axes 1-2 in eq. (33). Symmetric plies are combined because only a membrane load is considered and the strain in the material axes are constant through the thickness, so once the computation is done for a definite ply configuration, the rest of the plies with the same configuration will have identical value, hence

$$\begin{Bmatrix} e_1 \\ e_2 \\ e_{12} \end{Bmatrix} = \begin{bmatrix} cos^2\theta & sin^2\theta & cos\theta sin\theta \\ sin^2\theta & cos^2\theta & -cos\theta sin\theta \\ -2cos\theta sin\theta & 2cos\theta sin\theta & (cos^2\theta - sin^2\theta) \end{bmatrix} \begin{Bmatrix} e_x \\ e_y \\ e_{xy} \end{Bmatrix} (33)$$

For plies 1 and 6 at 30°

$$\begin{Bmatrix} e_1 \\ e_2 \\ e_{12} \end{Bmatrix} = \begin{bmatrix} 0.75 & 0.25 & 0.433013 \\ 0.25 & 0.75 & -0.43301 \\ -0.86603 & 0.866 & 0.5 \end{bmatrix} \begin{Bmatrix} 0.003998 \\ -0.001117 \\ 0 \end{Bmatrix}$$

$$\begin{Bmatrix} e_1 \\ e_2 \\ e_{12} \end{Bmatrix} = \begin{Bmatrix} 0.002719 \\ 0.000162 \\ -0.00443 \end{Bmatrix}$$

For plies 2 and 5 at 45^o

$$\begin{Bmatrix} e_1 \\ e_2 \\ e_{12} \end{Bmatrix} = \begin{bmatrix} 0.5 & 0.5 & 0.5 \\ 0.5 & 0.5 & -0.5 \\ -1 & 1 & 0 \end{bmatrix} \begin{Bmatrix} 0.003998 \\ -0.001117 \\ 0 \end{Bmatrix}$$

$$\begin{Bmatrix} e_1 \\ e_2 \\ e_{12} \end{Bmatrix} = \begin{Bmatrix} 0.001441 \\ 0.001441 \\ -0.00512 \end{Bmatrix}$$

For plies 3 and 4 at 90^o

$$\begin{Bmatrix} e_1 \\ e_2 \\ e_{12} \end{Bmatrix} = \begin{bmatrix} 3.75\text{E}-33 & 1 & 6.13\text{E}-17 \\ 1 & 3.8\text{E}-33 & -6.1\text{E}-17 \\ -1.2\text{E}-16 & 1.2\text{E}-16 & -1 \end{bmatrix} \begin{Bmatrix} 0.003998 \\ -0.001117 \\ 0 \end{Bmatrix}$$

$$\begin{Bmatrix} e_1 \\ e_2 \\ e_{12} \end{Bmatrix} = \begin{Bmatrix} -0.00112 \\ 0.003998 \\ -6.3\text{E}-19 \end{Bmatrix}$$

3.3.1.2. *Computation of PEFBFL ply stresses in material axes:*

The ply stresses in the material axis is related to the ply strains in the material axes as shown in eq. (34).

$$\begin{Bmatrix} \sigma_1 \\ \sigma_2 \\ \tau_{12} \end{Bmatrix} = \begin{Bmatrix} \frac{E_1}{1-v_{12}v_{21}} & \frac{v_{21}E_1}{1-v_{12}v_{21}} & 0 \\ \frac{v_{12}E_2}{1-v_{12}v_{21}} & \frac{E_2}{1-v_{12}v_{21}} & 0 \\ 0 & 0 & G_{12} \end{Bmatrix} \begin{Bmatrix} e_1 \\ e_2 \\ e_{12} \end{Bmatrix} \quad (34)$$

Therefore the ply strains in material axes 1-2 for each ply are used to establish the stress-strain relationship as follows:

For plies 1 and 6 at 30^o

$$\begin{Bmatrix} \sigma_1 \\ \sigma_2 \\ \tau_{12} \end{Bmatrix} = \begin{Bmatrix} 16011.07 & 2865.98 & 0 \\ 2866.76 & 7544.11 & 0 \\ 0 & 0 & 3622.99 \end{Bmatrix} \begin{Bmatrix} 0.00271929 \\ 0.0001618 \\ -0.00443 \end{Bmatrix}$$

$$\begin{Bmatrix} \sigma_1 \\ \sigma_2 \\ \tau_{12} \end{Bmatrix} = \begin{Bmatrix} 44.00 \\ 9.02 \\ -16.05 \end{Bmatrix}$$

For plies 2 and 5 at 45^o

$$\begin{Bmatrix} \sigma_1 \\ \sigma_2 \\ \tau_{12} \end{Bmatrix} = \begin{Bmatrix} 16011.07 & 2865.98 & 0 \\ 2866.76 & 7544.11 & 0 \\ 0 & 0 & 3622.99 \end{Bmatrix} \begin{Bmatrix} 0.00144054 \\ 0.0014405 \\ -0.005115 \end{Bmatrix}$$

$$\begin{Bmatrix} \sigma_1 \\ \sigma_2 \\ \tau_{12} \end{Bmatrix} = \begin{Bmatrix} 27.19 \\ 15.00 \\ -18.53 \end{Bmatrix}$$

For plies 3 and 4 at 90^o

$$\begin{Bmatrix} \sigma_1 \\ \sigma_2 \\ \tau_{12} \end{Bmatrix} = \begin{Bmatrix} 16011.07 & 2865.98 & 0 \\ 2866.76 & 7544.11 & 0 \\ 0 & 0 & 3622.99 \end{Bmatrix} \begin{Bmatrix} -0.001117 \\ 0.003998 \\ -6.27\text{E}-19 \end{Bmatrix}$$

$$\begin{Bmatrix} \sigma_1 \\ \sigma_2 \\ \tau_{12} \end{Bmatrix} = \begin{Bmatrix} -6.43 \\ 26.96 \\ 0.00 \end{Bmatrix}$$

Using the Maximum Principal Stress Theory which suggests that the ply will fail when any stress value in the material axes exceeds their respective ultimate strength. Such that

$$\left|\frac{\sigma_1}{S_{u1}}\right| < 1;\ \left|\frac{\sigma_2}{S_{u2}}\right| < 1;\ \left|\frac{\sigma_{12}}{\tau_{max}}\right| < 1 \quad (35)$$

The left hand side of eqs. (35) represents the strength ratio (SR). The maximum Strength ratio (SR) for the applied stress is factored in to obtain the load factor. Table 9 showed the ply stresses associated strength ratios at $N_x =$ 25N/mm for PEFBFL, it can be seen that maximum strength ratio of 0.9596 occured in ply 2 at 45 degrees in shear mode. Therefore at $N_x =$ 25N/mm no ply failure has yet occurred, hence the load intensity that can cause first ply to fail according to Maximum Principal Stress Theory in the 45 degree plies in shear mode is $N_x = \frac{25}{0.95969} = 26$ N/mm, furthermore, since the laminate is symmetric with membrane load only, the failure of ply two and ply five are predicted simultaneously. Similar computations were carried out for PPSFL and result presented in Table 10.

Table 9: Ply stresses and associated strength ratios in PEFBFL @ $N_x = 25$ (N/mm) and $E_x = 9649.789$ (N/mm^2)

ply	θ	e1	e2	e12	σ1	σ2	σ12	SR.1	SR.2	SR.12
1	30	0.002719	0.00016	-0.00443	44.002	9.0161	-16.048	0.1073	0.2411	0.83112
2	45	0.001441	0.00144	-0.00513	27.19	15.00	-18.53	0.0663	0.4009	0.95969
3	90	-0.00112	0.00399	-6.26E-19	-6.43	26.96	0.00	0.01567	0.7208	1.2E-16
4	90	-0.00112	0.00399	-6.27E-19	-6.43	26.96	0	0.01567	0.7208	1.20E-16
5	45	0.001441	0.00144	-0.00512	27.19	15	-18.53	0.0663	0.4009	0.95969
6	30	0.002719	0.00016	-0.00443	44.002	9.0161	-16.048	0.1073	0.2411	0.83112

Table 10: Ply stresses and associated strength ratios in PPSFL @ $N_x = 25$(N/mm) and $E_x = 8736.345$ (N/mm^2)

ply	θ	e1	e2	e12	σ1	σ2	σ12	SR.1	SR.2	SR.12
1	30	0.00144	0.00014	-0.00225	20.146	4.0099	-7.5124	0.04912	0.10722	0.38904
2	45	0.00079	0.00079	-0.00260	14.92	8.23	-9.43	0.03638	0.22003	0.48834
3	90	-0.0005	0.00209	-3.19E-19	-2.19	14.32	0.00	0.00533	0.38278	6.0E-17
4	90	-0.0005	0.00209	-3.19E-19	-2.19	14.32	0	0.00533	0.38278	6.0E-17
5	45	0.00079	0.00079	-0.00260	14.92	8.23	-9.43	0.03638	0.2200	0.48834
6	30	0.00144	0.00014	-0.00225	20.146	4.0099	-7.5124	0.04912	0.10721	0.38904

Table 11: $\bar{Q}_{ij}$ values (N/mm^2) for PEFBFL when ply 2 and 5 has completely failed

Ply	θ (Degree)	$\bar{Q}_{11}$	$\bar{Q}_{22}$	$\bar{Q}_{33}$	$\bar{Q}_{12}$	$\bar{Q}_{13}$	$\bar{Q}_{23}$
1	30	13269.72	9036.24	4247.60	3490.59	2193.77	1472.53
2	45	0	0	0	0	0	0
3	90	7544.11	16011.07	3622.99	2865.98	0	0
4	90	7544.11	16011.07	3622.99	2865.98	0	0
5	45	0	0	0	0	0	0
6	30	13269.72	9036.24	4247.6	3490.59	2193.77	1472.53

3.3.2 Second-ply-failure analysis

For second-ply-failure analysis, it is assumed that all the elastic values E_1, E_2 and G_{12} for the two already failed plies 2 and 5 are zero; hence the reduced and transformed reduced stiffness for plies 2 and 5 are zero. Therefore the new assumed transformed reduced stiffness term for PEFBFL is presented in Table 11.

The altered laminate configuration shown in Table 11 is still symmetric, so considering only membrane load, a partially populated compliance matrices is obtained from eq. 24. Computed ply strain and stresses in material axes is shown in Table 12, the ply stresses in the material axis is related to the ply strains in the material axes as shown in eq. 34. The ply strain in material axes 1-2 for each ply is hence used to establish the stress-strain relationship. Table 12 showed the ply stresses and associated strength ratios in PEFBFL at $N_x = 26$N/mm, it can be seen that maximum strength ratio of 1.27715 occured in ply 1 at 6 at 30 degrees in shear mode. Therefore at $N_x = 26$N/mm ply 1 at 6 failure has occured, furthermore, since the laminate is symmetric with membrane load only, the failure of ply one and ply six are predicted simultaneously.

Table 13 showed the ply stresses and associated strength ratios in PPSFL at $N_x = 26$N/mm, it can be seen that maximum strength ratio of 0.59418 occurred in ply 1 at 6 at 30 degrees in shear mode. Therefore at $N_x = 26$N/mm no subsequent ply failure has occured in this reduced stiffness laminate, therefore the load to cause the ply failure according to Maximum Principal Stress Theory in 30 degree plies in shear mode is $N_x = {}^{26}/_{0.59418} = 44$ N/mm.

3.3.3 Third-ply-failure analysis

For Third-ply-failure analysis, it is assumed that all the elastic values E_1, E_2 and G_{12} for the four failed plies 1, 2, 5 and 6 are zero, hence the reduced and transformed reduced stiffness for plies 1, 2, 5 and 6 are zero. Thus the new transformed reduced stiffness terms for the composite are presented in Table 14.

Table 12: Ply stresses and associated strength ratios in PEFBFL @ $N_x = 26$(N/mm) and $E_x = 6400.214$(N/mm^2)

ply	θ	e1	e2	e12	σ1	σ2	σ12	SR.1	SR.2	SR.12
1	30	0.00430	0.00037	-0.0068	69.9847	15.1605	-24.66	0.1706	0.4054	1.2771
2	45	0	0	0	0	0	0	0	0	0
3	90	-0.00159	0.00627	-9.6E-19	-7.51	42.73	0	0.0183	1.1426	1.8E-16
4	90	-0.00159	0.00627	-9.6E-19	-7.51	42.73	0	0.0183	1.1426	1.8E-16
5	45	0	0	0	0	0	0	0	0	0
6	30	0.004304	0.00037	-0.0068	69.9847	15.1605	-24.66	0.1706	0.4054	1.2771

Table 13: Ply stresses and associated strength ratios in PPSFL @ $N_x = 26$ (N/mm) and $E_x = 5826.376$(N/mm^2)

ply	θ	e1	e2	e12	σ1	σ2	σ12	SR.1	SR.2	SR.12
1	30	0.00227	0.00028	-0.00344	31.8576	6.7477	-11.474	0.0777	0.1804	0.594
2	45	0	0	0	0	0	0	0	0	0
3	90	-0.0007	0.00326	-4.87E-19	-2.07	22.56	0.00	0.0051	0.6033	9.1E-17
4	90	-0.0007	0.00326	-4.87E-19	-2.07	22.56	0	0.0051	0.6033	9.10E-17
5	45	0	0	0	0	0	0	0	0	0
6	30	0.00227	0.00028	-0.00344	31.8576	6.7477	-11.474	0.0777	0.1804	0.594

Table 14: $\bar{Q}_{ij}$ values (N/mm^2) for PEFBFL when ply 1, 2, 5 and 6 has completely failed

Ply	θ	$\bar{Q}_{11}$	$\bar{Q}_{22}$	$\bar{Q}_{33}$	$\bar{Q}_{12}$	$\bar{Q}_{13}$	$\bar{Q}_{23}$
1	30	0	0	0	0	0	0
2	45	0	0	0	0	0	0
3	90	7544.11	16011.07	3622.99	2865.98	0	0
4	90	7544.11	16011.07	3622.99	2865.98	0	0
5	45	0	0	0	0	0	0
6	30	0	0	0	0	0	0

The altered laminate configuration shown in Table 14 is still symmetric, so considering only membrane load, a partially populated compliance matrices is obtained from eq. (19). Following the method used in first and second ply failure analysis, the ply stresses and associated strength ratios at $N_x = 26$N/mm, is shown in Table 15. It can be seen that maximum strength ratio of 3.218395 occured in ply 3 and 4 at 90 degrees in tensile mode of transverse direction. Therefore at $N_x = 26$N/mm ply failure has occured in PEFBFL, furthermore, since the laminate is symmetric with membrane load only, the failure of ply one and six are predicted simultaneously.

Similarly for PPSFL, it can be seen in Table 16 that maximum strength ratio of 2.690382 occurred in ply 3 and 4 at 90 degrees in tensile mode of transverse direction. Therefore at $N_x = 44$N/mm ply failure has occured in PPSFL, furthermore, since the laminate is symmetric with membrane load only, the failure of ply one and six are predicted simultaneously.

The average stress which is the overall laminate strength (σ_x) is therefore failure load divided by laminate thickness which is $\sigma_x = {}^{N_x}/_{t} = {}^{26}/_{0.648} = 40.12\ \text{N/mm}^2$ for PEFBFL. While PPSFL is $\sigma_x = {}^{N_x}/_{t} = {}^{44}/_{1.368} = 32.16\ {}^{\text{N}}/_{\text{mm}^2}$. Eq. (31) gives the corresponding strain $e_x$at each ply failure as $e_x = \frac{N_x L_{22}}{LL}$ because $N_x = N_{xy} = 0$.

4. Conclusions

Based on the macro-mechanical analysis of $(30/45/90)_s$ laminate under tensile loading, the following conclusions are drawn:

1. Higher number of layer contributes to increased strength and stiffness in multi-oriented natural fiber/polyester laminate.

Table 15: Ply stresses and associated strength ratios in PEFBFL @ $N_x = 26$ (N/mm) and $E_x = 2343.699(\text{N/mm}^2)$

ply	θ	e1	e2	e12	σ1	σ2	σ12	SR.1	SR.2	SR.12
1	30	0	0	0	0	0	0	0	0	0
2	45	0	0	0	0	0	0	0	0	0
3	90	-0.00306	0.01712	-2.473E-18	0.00	120.37	0.00	0	3.218395	4.6E-16
4	90	-0.00306	0.01712	-2.47E-18	0	120.37	0	0	3.218395	4.60E-16
5	45	0	0	0	0	0	0	0	0	0
6	30	0	0	0	0	0	0	0	0	0

Table 16: Ply stresses and associated strength ratios in PPSFL @ $N_x = 44$ (N/mm) and $E_x = 2272.221(\text{N/mm}^2)$

Ply	θ	e1	e2	e12	σ1	σ2	σ12	SR.1	SR.2	SR.12
1	30	0	0	0	0	0	0	0	0	0
2	45	0	0	0	0	0	0	0	0	0
3	90	-0.00215	0.0141552	-1.998E-18	6.12	100.62	0.00	0.01492	2.690382	3.7E-16
4	90	-0.00215	0.0141552	-2.00E-18	6.12	100.62	0	0.01492	2.690382	3.70E-16
5	45	0	0	0	0	0	0	0	0	0
6	30	0	0	0	0	0	0	0	0	0

Table 17: The average values of stress (σ_x) and strain (e_x) for PEFBFL and PPSFL

Ply	PEFBFL					PPSFL				
	N_x	$\frac{L_{22}}{LL}$	e_x (%)	σ_x (N/mm²)	Displ. (mm)	N_x	$\frac{L_{22}}{LL}$	e_x (%)	σ_x (N/mm²)	Displ. (mm)
1	25	0.00016	0.0039	38.5803	0.001	25	0.00008	0.0021	18.27485	0.000523
2	26	0.00021	0.0063	40.1235	0.00157	26	0.00013	0.0034	19.00585	0.000815
3	26	0.00039	0.0171	40.1235	0.00428	44	0.00032	0.0142	32.16374	0.00355

Table 18: The values of stress (σ_x) and deformation for PEFBFL and PPSFL

COMPOSITE	σ_x (N/mm²)			Displacement (mm)		
	CLT	ANN	%Error	CLT	ANN	%Error
PEFBFL	40.1235	40.1298	1.23	0.00428	0.004151	3.01
PPSFL	32.1637	32.5589	1.23	0.00355	0.00358	0.85

2. The laminate equivalent elastic constants (E_x, E_y, G_{xy} , v_{xy} , y_{yx} , m_x and m_y) for symmetric plantain fiber/polyester laminate have been determined in membrane and bending modes.

3. The maximum principal stress theory provided the necessary sets of physics-based failure criteria for predicting the plantain fiber/polyester laminate failure using the lamina-based longitudinal, transverse and shear strengths.

4. A steady reduction in the laminate elastic modulus was observed as a result of compromised stiffness in principal directions arising from gradual failure of the plies until the last ply failure occurred in ply 3 and 4 at 90 degrees in tensile mode of transverse direction.

5. Stresses and displacements observed in the symmetric plantain fiber/polyester laminate with specified mechanical loading condition using Classical Laminate Theory agree very closely with predictions of ANN.

6. The urgency of a fast technique that simulates macro-mechanical characteristics of laminate can be fulfilled by using an artificial neural network trained with raw experimental data obtained from finite element analysis in the range of loads and material control factors studied.

7. Considering the rich micro-structural information gathered from this stiffness and macroscopic analysis, it is believed that this technique deserves further study as an initial screening mechanism in advanced composite development programmes.

Acknowledgements

The supportive role played by Nnamdi Azikiwe University Awka in providing enabling environment for this research is highly acknowledged.

Appendix

Table 19: The ANN training data set and response for PEFBFL

	Independent variables			Response 1			Response 2		
Exp No.	Aspect Ratio	Fiber Orientation	Stacking Sequence	Stress (N/mm²)	ANN Predicted	Error	Displacement (mm)	ANN Predicted	Error
1	1.05	60	(30/0/90)s	37.13	36.6834	0.44660	0.00361	0.003614	-3.87E-06
2	0.79	30	(30/0/90)s	36	36.1061	-0.10615	0.00315	0.003172	-2.18E-05
3	1.05	60	(30/45/90)s	40.13	40.0192	0.110736	0.00423	0.004121	0.00010879
4	1.05	60	(30/45/90)s	40.13	40.0192	0.110736	0.00423	0.004121	0.00010879
5	1.05	60	(30/45/90)s	40.13	40.0192	0.110736	0.00423	0.004121	0.00010879
6	1.05	60	(30/0/90)s	36.13	36.6834	-0.5534	0.00299	0.003614	-0.0006239
7	0.68	60	(30/0/90)s	34.5	34.5005	-0.00053	0.00259	0.002606	-1.61E-05
8	1.42	60	(30/45/90)s	39.13	40.0247	-0.89474	0.00423	0.004198	3.15E-05
9	1.31	90	(30/0/90)s	38	39.8442	-1.84425	0.00423	0.004191	3.88E-05
10	1.05	90	(30/45/90)s	40.13	40.1295	0.000424	0.00423	0.004193	3.68E-05
11	1.31	30	(30/0/90)s	34.8	34.8637	-0.06373	0.00315	0.003485	-0.000335
12	1.05	90	(30/0/90)s	36.6	36.6394	-0.03941	0.00353	0.003546	-1.63E-05
13	1.05	60	(30/0/90)s	37.13	36.6834	0.446604	0.00315	0.003614	-0.000464
14	1.05	60	(30/0/90)s	37.13	36.6834	0.446604	0.00423	0.003614	0.00061613
15	0.79	90	(30/45/90)s	40.13	40.1281	0.0019	0.00423	0.003945	0.00028501
16	1.31	90	(30/45/90)s	40.13	40.1298	0.000107	0.00423	0.004151	7.92E-05
17	1.05	60	(30/45/90)s	38.13	40.0193	-1.88926	0.00423	0.004121	0.00010879
18	1.42	60	(30/0/90)s	37.13	37.1604	-0.03047	0.00423	0.004207	2.35E-05
19	0.79	30	(30/45/90)s	38.8	38.6298	0.170174	0.00315	0.003135	1.46E-05
20	0.68	60	(30/45/90)s	37.13	37.1190	0.010906	0.00259	0.002642	-5.22E-05
21	1.05	30	(30/0/90)s	35.8	35.7035	0.096432	0.00323	0.003332	-0.000102
22	0.79	90	(30/0/90)s	35	34.9949	0.0051	0.00315	0.003176	-2.64E-05
23	1.05	60	(30/45/90)s	40	40.0192	-0.01926	0.00422	0.004121	9.88E-05
24	1.05	60	(30/0/90)s	37.13	36.6834	0.446604	0.00323	0.003614	-0.000384
25	1.31	30	(30/45/90)s	38	37.9603	0.039629	0.00323	0.003255	-2.48E-05
26	1.05	30	(30/45/90)s	38	38.4618	-0.46185	0.00323	0.003163	6.69E-05
					Σ	-3.45975		Σ	-3.44E-04
					MSE=	0.46038		MSE=	4.5544E-09

Code value: (30/0/90)s =>1, (30/45/90)s=>2

Table 20: The ANN training data set and response for PPSFL

Independent variables				Response 1			Response 2		
Exp No.	Aspect Ratio	Fiber Orientation	Stacking Sequence	Stress (N/mm^2)	ANN Predicted	Error	Displacement (mm)	ANN Predicted	Error
1	1.05	60	(30/0/90)s	27.13	28.44332	-1.31332	0.00261	0.002682	-7.23E-05
2	0.79	30	(30/0/90)s	26	26.0954	-0.0954	0.00215	0.002161	-1.07E-05
3	1.05	60	(30/45/90)s	32.61	31.83736	0.772644	0.00358	0.003508	7.15E-05
4	1.05	60	(30/45/90)s	32.61	31.83736	0.772644	0.00358	0.003508	7.15E-05
5	1.05	60	(30/45/90)s	32.61	31.83736	0.772644	0.00358	0.003508	7.15E-05
6	1.05	60	(30/0/90)s	28.13	28.44332	-0.31332	0.00299	0.002682	0.00030771
7	0.68	60	(30/0/90)s	26.5	26.18098	0.319022	0.00259	0.002401	0.00018924
8	1.42	60	(30/45/90)s	29.13	28.94753	0.182469	0.00358	0.003572	7.83E-06
9	1.31	90	(30/0/90)s	30	30.00286	-0.00286	0.00358	0.003142	0.00043795
10	1.05	90	(30/45/90)s	32.61	32.21414	0.395862	0.00358	0.003573	7.08E-06
11	1.31	30	(30/0/90)s	26.8	26.78153	0.018465	0.00215	0.002192	-4.22E-05
12	1.05	90	(30/0/90)s	28.6	28.5736	0.026401	0.00253	0.002878	-0.000348
13	1.05	60	(30/0/90)s	29.13	28.44332	0.686676	0.00215	0.002682	-0.0005323
14	1.05	60	(30/0/90)s	29.13	28.44332	0.686676	0.00358	0.002682	0.00089771
15	0.79	90	(30/45/90)s	29	29.04575	-0.04575	0.00258	0.002687	-0.00011
16	1.31	90	(30/45/90)s	32.61	32.55896	0.051038	0.00358	0.003578	1.93E-06
17	1.05	60	(30/45/90)s	30.13	31.83736	-1.70736	0.00358	0.003508	7.15E-05
18	1.42	60	(30/0/90)s	29.13	28.69715	0.432848	0.00358	0.003407	0.00017295
19	0.79	30	(30/45/90)s	30.8	30.7556	0.044397	0.00255	0.002387	0.00016264
20	0.68	60	(30/45/90)s	29.13	29.62188	-0.49188	0.00259	0.002551	3.94E-05
21	1.05	30	(30/0/90)s	27.8	27.62689	0.173107	0.00223	0.002223	6.65E-06
22	0.79	90	(30/0/90)s	26	26.18772	-0.18772	0.00215	0.002291	-0.0001414
23	1.05	60	(30/45/90)s	32	31.83736	0.162644	0.00322	0.003508	-0.0002885
24	1.05	60	(30/0/90)s	29.13	28.44332	0.686676	0.00223	0.002682	-0.000452
25	1.31	30	(30/45/90)s	30	27.88602	2.113975	0.00223	0.002957	-0.0007266
26	1.05	30	(30/45/90)s	30	30.01162	-0.01162	0.00223	0.002206	2.38E-05
					Σ	4.128949		Σ	-1.81E-04
					MSE=	0.655701		MSE=	1.2577E-09

Code value: (30/0/90)s =>1, (30/45/90)s=>2

References

[1] Rijswijk, K. V., Brouwer, W. D., & Beukers, A. 2001. Application of natural fibre composites in the development of rural societies. Structures and Materials Laboratory Faculty of Aerospace Engineering. Retrieved May 10, 2020, from http://www.fao.org/3/ad416e/ad416e00.htm

[2] Kılınç, A. Ç., Durmuşkahya, C., & Seydibeyoğlu, M. Ö. 2017. Natural fibers. In *Fiber Technology for Fiber-Reinforced Composites* (pp. 209-235). Woodhead Publishing.

[3] Peças, P., Carvalho, H., Salman, H., & Leite, M. 2018. Natural fibre composites and their applications: a review. *Journal of Composites Science*, *2*(4), 66.

[4] Moore S. 2019. *Improving Bridge Construction with Fiber-Reinforced Polymers*. Retrieved May 10, 2020, from https://www.azobuild.com/article.aspx?ArticleID=8363

[5] Ihueze, C., Oluleye, A., Okafor, C. E., Obele, C., Abdulrahman, J., & Obuka, S. 2017. Development of plantain fibres for application in design of oil and gas product systems. *Petroleum Technology Development Journal: An International Journal*, *7*(1).

[6] Beauson, J., Madsen, B., Toncelli, C., Brøndsted, P., & Bech, J. I. 2016. Recycling of shredded composites from wind turbine blades in new thermoset polymer composites. *Composites Part A: Applied Science and Manufacturing*, *90*, 390-399.

[7] Amanda J. 2010.*Composite panels enable fast house construction*. Retrieved May 10, 2020, from https://www.materialstoday.com/composite-applications/news/composite-panels-enable-fast-house-construction/

[8] Rajak, D. K., Pagar, D. D., Kumar, R., & Pruncu, C. I. 2019. Recent progress of reinforcement materials: a comprehensive overview of composite materials. *Journal of Materials Research and Technology*, 8(6), 6354-6374.

[9] Noora, K. 2017. *Telecommunications: Composite enablers for future smart cities*. Retrieved May 10, 2020 from https://news.cision.com/exel-composites/r/telecommunications--composite-enablers-for-future-smart-cities,c2328270

[10] Patel, J. P., & Parsania, P. H. 2018. Characterization, testing, and reinforcing

materials of biodegradable composites. In *Biodegradable and biocompatible polymer composites* (pp. 55-79). Woodhead Publishing United Kingdom.

[11] Imoisili, P. E., Fadare, O. B., Popoola, A. V., & Okoronkwo, A. E. 2017. Effect of chemical treatment on the morphology and mechanical properties of plantain (Musa paradisiaca) fibre. *IOSR Journal of Applied Chemistry*., 10(5), 70–73, https://doi.org/10.9790/5736-1005017073

[12] Widsten, P, & Kandelbauer, A 2008. Adhesion improvement of lignocellulosic products by enzymatic pre-treatment. *Biotechnology Advances*, *26*(4), 379-386.

[13] Madsen, B., & Gamstedt, E. K. 2013. Wood versus plant fibers: similarities and differences in composite applications. *Advances in Materials Science and Engineering*, 564346. 1-14.

[14] Adewole, S. 2017. Plantain (Musa acuminata) value chain analysis in Ondo State, Nigeria. *Scientific Papers: Management, Economic Engineering in Agriculture & Rural Development*, *17*(3).

[15] Okafor, C. E., Ihueze, C. C., & Nwigbo, S. C., 2013. Optimization of hardness strengths response of plantain fibres reinforced polyester matrix composites (PFRP) applying Taguchi robust design. *International journal of engineering*, *26*(1), 1-12.

[16] Ihueze, C. C., Okafor, C. E., & Okoye, C. I. 2015. Natural fiber composite design and characterization for limit stress prediction in multiaxial stress state. *Journal of King Saud University-Engineering Sciences*, *27*(2), 193-206.

[17] Okafor, C. E., & Godwin, H. C. 2014. Evaluation of compressive and energy adsorption characteristics of plantain fiber reinforced composites. *World Journal of Engineering and Physical Sciences*, *2*(3), 036-048.

[18] Ihueze, C. C., & Okafor, C. E. 2016. Optimal design for flexural strength of plantain fibers reinforced polyester matrix. *Journal of Innovative Research in Engineering and Sciences*, *4*(4). 520-537

[19] Cadena-Ch, E. M., Vélez R, J. M., Santa, J. F., & Otálvaro G, V. 2017. Natural fibers from plantain pseudostem (Musa paradisiaca) for use in fiber-reinforced composites. *Journal of Natural Fibers*, *14*(5), 678-690.

[20] Oreko, B. U., Otanocha, O. B., Emagbere, E., &Ihueze, C. C. 2018. Analysis and Application of Natural Fiber Reinforced Polyester Composites to Automobile Fender. *Covenant Journal of Engineering Technology (Special Edition)*, *1*(1).

[21] Adeniyi, A. G., Ighalo, J. O., & Onifade, D. V. 2019. Banana and plantain fiber-reinforced polymer composites. *Journal of Polymer Engineering*, *39*(7), 597-611.

[22] Imoisili, P. E., Ukoba, K., & Jen, T. C. 2020. Physical, mechanical and thermal properties of high frequency microwave treated plantain (Musa Paradisiaca) fibre/MWCNT hybrid epoxy nanocomposites. *Journal of Materials Research and Technology*. 9(3), 4933-4939

[23] Ye, J. 2002. *Laminated composite plates and shells: 3D modelling*. Springer Science & Business Media.

[24] Khandan, R., Noroozi, S., Sewell, P., Vinney, J., & Koohgilani, M. 2012. Optimum design of fibre orientation in composite laminate plates for out-plane stresses. *Advances in Materials Science and Engineering*, *2012*.

[25] Singh, C. V. 2016. Evolution of multiple matrix cracking. In *Modeling Damage, Fatigue and Failure of Composite Materials* (pp. 143-171). Woodhead Publishing.

[26] Hyer, M. W., & White, S. R. 2009. *Stress analysis of fiber-reinforced composite materials*. DEStech Publications, Inc.

[27] Vnučec, Z. 2005. Analysis of the laminated composite plate under combined loads. In *RIM 2005: 5th International Scientific Conference on Production Engineering*.

[28] Melro A. R 2011. *Analytical and numerical modelling of damage and fracture of advanced composites* (Doctoral dissertation, University of Porto (Portugal)).

[29] Kaw, A. K. 2005. *Mechanics of composite materials*. CRC press.

[30] Gibson, R. F. 2016. *Principles of composite material mechanics*. CRC press.

[31] Ahmad, F., & Bajpai, P. K. 2018. Evaluation of stiffness in a cellulose fiber reinforced epoxy laminates for structural applications: Experimental and finite element analysis. *Defence Technology*, *14*(4), 278-286.

[32] Rahimi, N., Hussain, A. K., Meon, M. S., & Mahmud, J. 2012. Capability assessment of finite element software in predicting the last ply failure of composite laminates. *Procedia Engineering*, *41*, 1647-1653.

[33] Saxena, M., &Kirtania, S. 2016. Stiffness analysis of symmetric cross-ply laminated composite plates. *ADBU Journal of Engineering Technology*, 4(1),76-81.

[34] Gantasala, K. C., & Kotkunde, N. 2017. Theoretical and finite element investigation of inter-laminar stresses for laminated

composite beam. *Materials Today: Proceedings*, *4*(8), 7731-7740.

[35] Abhishek J. 2015. First Ply Failure Analysis of Laminated Composite Plates on ANSYS Mechanical APDL. *International Journal of Engineering and Technical Research (IJETR),* 3(7), 237- 240.

[36] Rahul P. & Amit T. 2015. Analysis of Cross-ply Laminate composite under UD load based on CLPT by Ansys APDL. *Int. Journal of Engineering Research and Applications*, 5(9), 90-94

[37] Goswami, Y., & Saxena, R. 2016. Stress and failure analysis of inter-ply hybrid laminated composite using finite element method. *J. Eng. and Technol*, *3*(7), 2391-2396.

[38] Yosri, A. M., Ghanem, G. M., Salama, M. A., & Ehab, A. 2019. Structural performance of laminated composite thin-walled beams under four-point bending. *Innovative Infrastructure Solutions*, *4*(1), 58.

[39] Moheimani, R., Sarayloo, R., & Dalir, H. 2020. Failure study of fiber/epoxy composite laminate interface using cohesive multiscale model. *Advanced Composites Letters*, *29*, 2633366X20910157.

[40] Bogetti, T.A., Hoppel, C.P.R. Harik, V.M. Newill, J.F. & Burns B.P. 2004. Predicting the nonlinear response and progressive failure of composite laminates. Compos Sci Technol, 64 (3–4), 329-342

[41] Vaziri, R., Olson, M.D. & Anderson D.L. 1991. A plasticity-based constitutive model for fibre-reinforced composite laminates J Compos Mater, 25 (5), 512-535

[42] Hsuan-Teh, H. U., & Lung-Shen, K. E. 2019. Constitutive modelling of composite laminates under uniaxial compression. *Chinese Journal of Aeronautics*, *32*(4), 938-947.

[43] Dimitrienko, Y. I. 2018. Universal models for effective constitutive relations of laminated composites with finite strains. In *Journal of Physics: Conference Series* (Vol. 1141, No. 1, p. 012098). IOP Publishing.

[44] RajanishM, Nanjundaradhya N. V, Ramesh S S. , Bhaskar P 2013.A Review Of Failure Of Composite Materials. International Journal of Engineering Research and Applications. 3(2),122-124.

[45] Hinton MJ, Kaddour AS, Soden PD (Eds) 2004. Failure criteria in fibrereinforcedpolymer composites: the world-wide failure exercise. Amsterdam: Elsevier;

[46] Soden, P. D., Kaddour, A. S., & Hinton, M. J. 2004. Recommendations for designers and researchers resulting from the world-wide failure exercise. In *Failure Criteria in Fibre-Reinforced-Polymer Composites* (pp. 1223-1251). Elsevier.

[47] Talreja, R. 2016. On Failure Theories for Composite Materials. In *Advanced Methods of Continuum Mechanics for Materials and Structures* (pp. 379-388). Springer, Singapore.

[48] Timoshenko, S. P., & Woinowsky-Krieger, S. 1959. *Theory of plates and shells*. McGraw-hill.

[49] Datoo, M. H. 1991. *Mechanics of fibrous composites*. New York, Elsevier Applied Science.